Reevaluation of near-infrared light propagation in the adult human head: implications for functional near-infrared spectroscopy

Yoko Hoshi
Miho Shimada
Chie Sato
Yoshinobu Iguchi
Tokyo Institute of Psychiatry
Department of Integrated Neuroscience
2-1-8 Kamikitazawa, Setagaya-ku
Tokyo 156-8585, Japan
E-mail: yhoshi@prit.go.jp

Abstract. Using both experimental and theoretical methods, we examine the contribution of different parts of the head to near-IR (NIR) signal. Time-resolved spectroscopy is employed to measure the mean optical path length (PL), and the absorption (μ_a) and reduced scattering (μ_s') coefficients in multiple positions of the human head. Monte Carlo simulations are performed on four-layered head models based on an individual magnetic resonance imaging (MRI) scan to determine μ_a and μ_s' in each layer of the head by solving inverse problems, and to estimate the partial path length in the brain (p-PL) and the spatial sensitivity to regions in the brain at the source-detector separation of 30 mm. The PL is closely related to the thickness of the scalp, but not to that of other layers of the head. The p-PL is negatively related to the PL and its contribution ratio to the PL is 5 to 22% when the differential path length factor is 6. Most of the signal attributed to the brain comes from the upper 1 to 2 mm of the cortical surface. These results indicate that the NIR signal is very sensitive to hemodynamic changes associated with functional brain activation in the case that changes in the extracerebral tissue are ignorable. [DOI: 10.1117/1.2142325]

Keywords: time-resolved spectroscopy; Monte Carlo simulation; partial path length; absorption coefficients; reduced scattering coefficients.

Paper 05049R received Feb. 22, 2005; revised manuscript received Jun. 20, 2005; accepted for publication Jul. 26, 2005; published online Dec. 30, 2005.

1 Introduction

While near-infrared spectroscopy (NIRS) has been oriented toward use for clinical monitoring of tissue oxygenation,[1,2] this technique is now developing into a useful tool for neuroimaging studies.[3,4] Since Jöbsis first described[5] the *in vivo* application of NIRS in 1977, several types of NIRS instruments, which are associated with an equally wide range of types of measurement, have been developed. The type of measurement made in the earliest clinical NIRS studies, which is employed in current commercially available instruments, is to measure the transmitted light intensity and calculated concentration changes in chromophores based on the modified Beer-Lambert law.[6] Instruments of this type (cw-type instruments) enable us to continuously measure hemoglobin (Hb) concentration changes accompanying changes in neuronal activity in real time. However, since cw-type instruments cannot measure the optical path length in tissue, quantification of Hb concentration changes is impossible. To solve the problem of data quantification, over the past 25 yr many different approaches have been tried, such as time-resolved spectroscopy[6,7] (TRS) and phase-resolved spectroscopy.[8,9]

In TRS, ultrashort (picosecond) pulsed light is input to the tissues and the emerging photons are detected as a function of time (the temporal point spread function, TPSF) with picosecond resolution. Multiplying light speed in the tissue by the mean time of flight of photons, which is estimated from the TPSF, provides the mean path length (PL) light travels between the source and detector. In the case where hemodynamic changes are global and homogeneous within the head, quantification is possible by substitution of the estimated PL into the modified Beer-Lambert law. When the changes are localized within the brain, as in functional brain activation, however, the estimated Hb concentration changes are smaller than the real concentration changes because[10] the partial path length in the brain (p-PL) is shorter than the PL (partial volume error). Only if the ratio of the p-PL to the PL is the same among measurement positions, which may hold when there is no positional difference in the PL, is it possible to compare amplitude of the NIRS signals among different subject groups and different measurement positions in a given subject. In a series of our studies with TRS, however, we found that positional variation of the PL is large at the lateral side of the head, though it is relatively small at the forehead. The PL was positively related to the reduced scattering coefficient (μ_s') of the head but not the absorption coefficient (μ_a) measured by

Address all correspondence to Yoko Hoshi, Integrated Neuroscience Research Team, Tokyo Institute of Psychiatry, 2-1-8 Kamikitazawa, Setagaya-ku, Tokyo 156-8585, Japan. Tel: 81–3–3304–5701. Fax: 81–3–3329–8035. E-mail: yhoshi@prit.go.jp

1083-3668/2005/10(6)/064032/10/$22.00 © 2005 SPIE

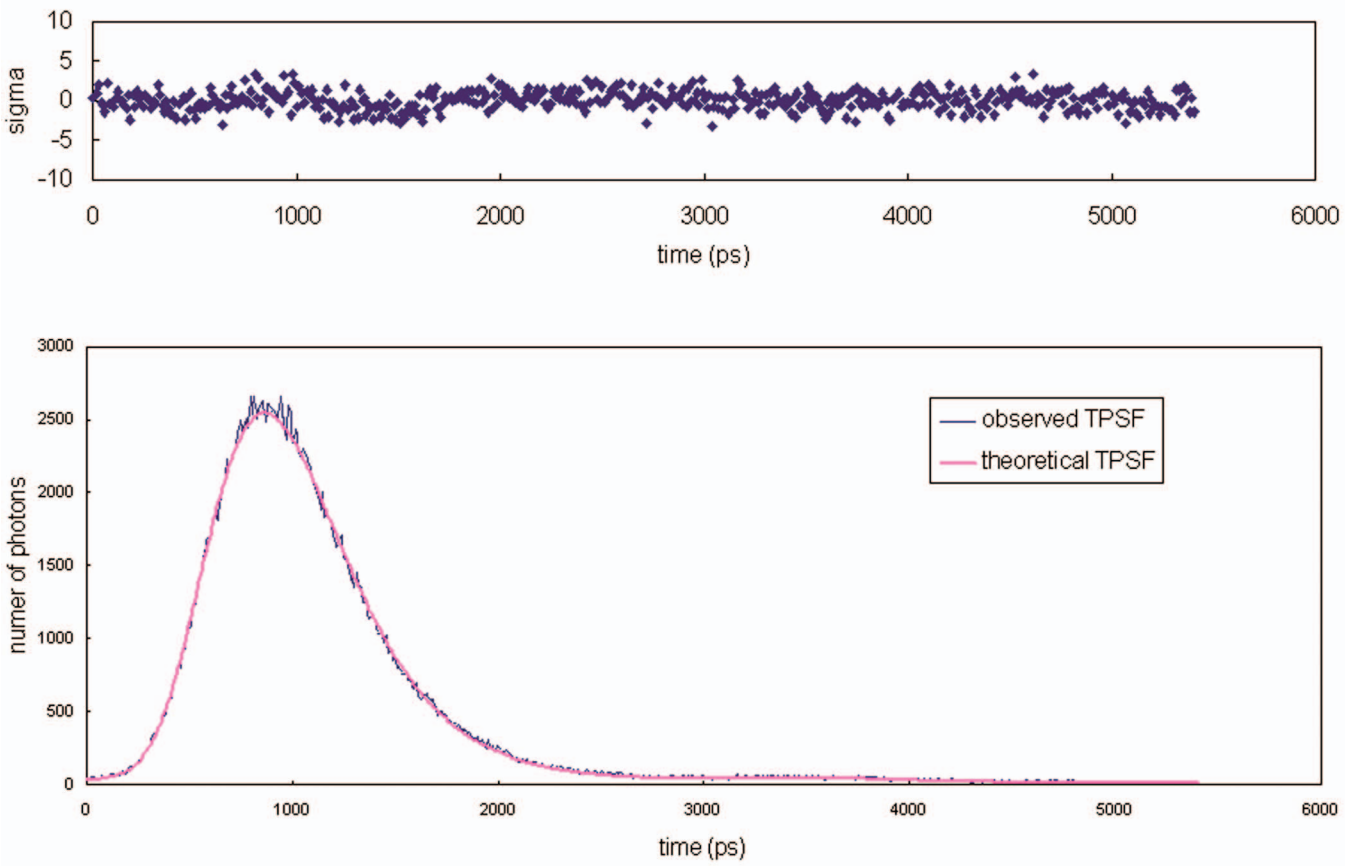

Fig. 1 Example of the curve-fitting data. The observed TPFC at 759 nm was obtained from measurements on the left forehead of a 23-year-old woman at a source detector spacing of 3 cm. Upper graph shows the weighted residuals.

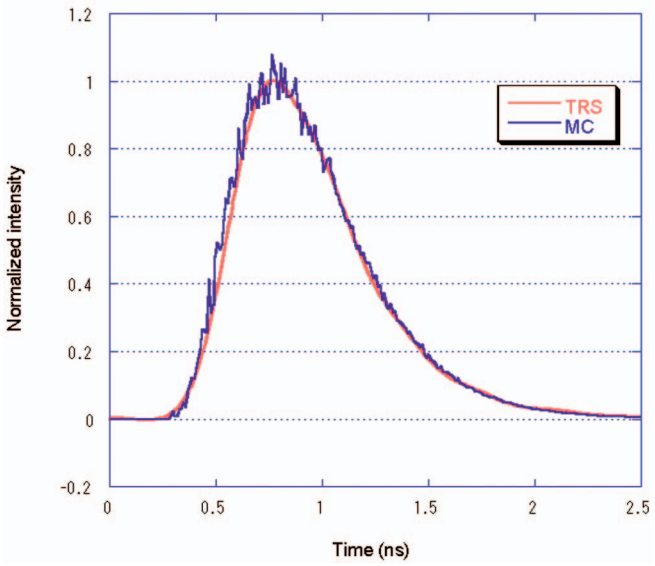

Fig. 5 TPSF obtained from the MC simulation and the deconvoluted TPSF obtained from the TRS measurement on subject 3.

TRS (data not shown). The μ_s' is determined mainly by the optical properties of the scalp and skull, while the μ_a is determined by the properties of the deeper region of the head, such as the brain.[11] The large positional variations of the PL were also observed by Zhao et al., who measured PL in the frontal, sensorimotor, and occipital regions with a multichannel TRS instrument.[12] They speculated that it was related to the thickness of the skull and muscle, which was not confirmed. Taken together, these results suggest that the detected light mainly propagates within the extracerebral tissue. Thus, the fundamental question arises: is NIR signal actually sensitive to changes associated with functional brain activation?

Although a number of theoretical and experimental investigations on NIR light propagation in the human head have been performed,[13–17] knowledge of which region in the brain is sampled by NIR light remains incomplete. Recent models for the theoretical analysis of light propagation in the head are based on an inhomogeneous structure. These models consist of multiple layers, such as the scalp, skull, cerebrospinal fluid (CSF), and the brain, which can be divided into the gray and white matters. In theoretical analysis, optical properties in each layer of the head are critical for prediction of the light propagation, though μ_a and μ_s' values in each layer used for analysis are different from study to study. This is attributable to the fact that *in situ* measurements of the optical properties are not feasible.

In this study, we employed both experimental and theoretical methods to examine the spatial sensitivity of the detected NIRS signal to different parts of the head. First, we measured the PL, μ_a and μ_s' in the human heads with TRS. Then, Monte Carlo simulations were used. To determine the optical properties of scalp, skull, CSF, and the brain, inverse problems with the four-layered model based on an individual magnetic resonance imaging (MRI) scan were solved using mean μ_a and mean μ_s' of the head measured by TRS. Using the determined optical properties of each layer, we examined the relationship between the PL and the p-PL, and estimated the depth sensitivity to cerebral hemodynamics.

2 Methods

2.1 *Subjects*

The subjects were 12 healthy adults (9 male, 3 female: age range, 21 to 48 yr; mean age, 24 yr). A written informed consent was obtained before the examination. One female subject was excluded from analysis of data because a subarachnoid cyst was found by chance in the MRI scan.

2.2 *Time-Resolved Spectroscopy Instrument*

A single-channel time-resolved spectroscopy instrument (TRS-10, Hamamatsu Photonics, Japan) was used in this study. The details of the TRS-10 have been described previously.[18] Briefly, the TRS-10 system consists of three pulsed laser diodes with different wavelengths (759, 797, and 833 nm) having a duration of around 100 ps at the repetition rate of 5 MHz, a high-speed photomultiplier tube (H6279-MOD) for single photon detection, and a circuit for time-resolved measurement based on the time-correlated single-photon-counting (TCSPC) method. The temporal profile of the emerging photons from the sample can be accumulated up to the count rate of 500 kcps at each wavelength simultaneously. But, to avoid the pile-up distortion, the temporal profiles are measured less than 150 kcps. Minimal data acquisition time is 100 ms. The instrumental response of the TRS-10 can be measured by placing the input fiber opposite to the detecting fiber through a neutral density filter. The instrumental response of the TRS-10 is about 150 ps FWHM at each wavelength.

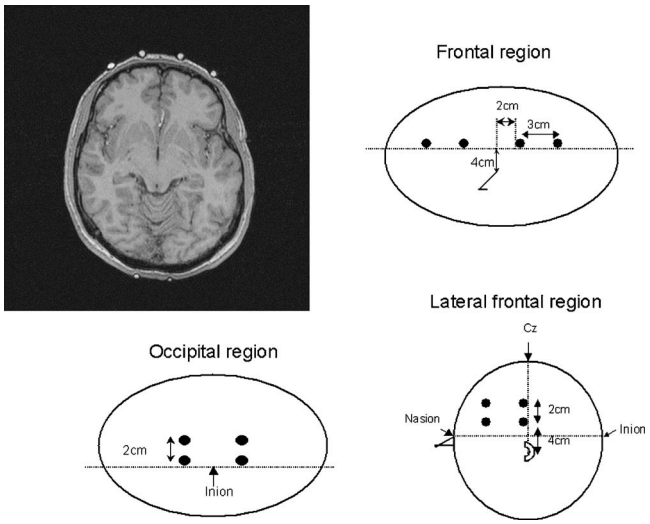

Fig. 2 Positions of spherical lipid markers (solid circle) placed on the head. The distance between two makers denotes the spacing from center to center.

The PL was calculated[19] by the simple subtraction method from the TPSF. The mean μ_a and mean μ_s' were estimated by fitting a theoretical TPSF (based on the solution of the photon diffusion equation[20] derived by employing the extrapolated boundary condition) to the observed TPSF (time range of 0 to 5400 ps). In the fitting procedure, a weighted least-squares fitting method based on Levenberg-Marquardt method, which is an iterative improvement method, was used since the TRS data measured by the TCSPC method have an error obeying a Poisson distribution. In each calculation, a function derived from the photon diffusion equation, which was convoluted with the instrumental response, was fitted into the observed TPSF. The refractive index in the human head was assumed to be 1.37. When the chi square nu (χ_ν^2) value was 0.7 to 1.3, we considered that the theoretical TPSF was well fitted to the observed one.[21,22] Here, we show an example of the curve-fitting data, which was arbitrarily chosen from data in our series of TRS studies. Figure 1 shows observed TPSF at 759 nm in the measurement on the forehead and theoretical TPSF and weighted residuals. In this case, the χ_ν^2 value is 1.16.

2.3 *MRI and TRS Measurements*

MRI scans (MAGNETOM System, Symphony 1.5 T, Siemens, slice thickness of 1.0 mm) were acquired with six pairs of spherical lipid markers placed on the head. The anatomical images of the head structure were obtained with an IR (inverse recovery) sequence (TR, 2200 ms; TE, 3.93 ms; resolution, 224×256 pixel). Figure 2 shows positions of the

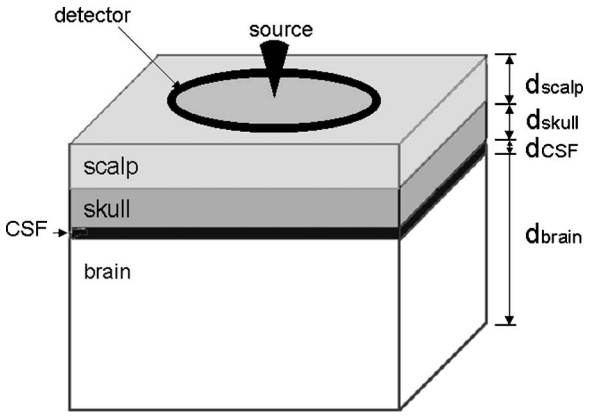

Fig. 3 Adult head model used in Monte Carlo simulation. The thickness of the scalp (d_{scalp}), skull (d_{skull}), and the CSF layer (d_{CSF}) were determined based on an individual MRI scan. The thickness of the brain (d_{brain}) was taken as the infinite.

markers. The distance between a pair of markers was 30 mm. The line between the nasion and inion was identified, and each pair of markers was placed so that they could be detected in the same axial slice. Thickness of the scalp, skull, temporal muscle, and CSF beneath the markers were measured and an averaged value between two positions was considered to be the thickness of each layer. Since the epicranical muscle is very thin, it is difficult to distinguish it from the scalp in MRI. Thus, we took both the scalp and epicranical muscle as the scalp.

After the MRI scan, time-resolved measurement was performed. Each subject sat in a chair in a quiet dark room with the eyelids open. The head was shielded from ambient light by a black cloth. The incident fiber (single fiber) with a core diameter of 200 μm and the detecting fiber [bundle fibers, numerical aperture (NA)=0.21] with a diameter of 3 mm were placed on the same head positions as those where each pair of markers was placed (source detector spacing of 30 mm). Acquisition and repetition time was set at 1 and 5 s, respectively.

2.4 *Monte Carlo Simulations*

2.4.1 *General approach*

To predict light propagation, determine the optical properties, and estimate the p-PLs, we performed Monte Carlo simulations on the adult head model. We used the Monte Carlo code developed by Wang and Jacques,[23] which was modified to correspond to our measurement system so that photons reaching the detector were counted every 10 ps and scattering events in a given layer were counted. The head model is a slab consisting of four layers that imitate the scalp, skull, CSF layer, and brain (Fig. 3). The thickness of the scalp, skull, and the CSF layer were determined based on an individual MRI scan. Incident photons were perpendicularly applied to the surface as a parallel beam and emerging photons were detected in concentric rings differing 3 mm in diameter. The middle ring radius of these rings was 28.5 mm. The calculation was repeated until the detected photon numbers reached 1,000,000 on the assumption that g (the mean cosine of the scattering angle) is 0 (isotropic scattering). A refractive index of 1.37 was used for all four layers. Reflectance and number of scattering events in layers ranging from z to $z+1$ mm in depth were counted every 10 ps.

Table 1 Initial values of Monte Carlo simulation parameters.

Layer	μ_a (mm^{-1})	μ_s' (mm^{-1})
Scalp	0.01	1.5
Skull	0.008	0.7
CSF	0.0033	0.1
Brain	0.02	1.0

2.4.2 *Estimation of optical properties for the scalp, skull, CSF, and brain (inverse problem)*

Two male subjects (subjects 1 and 2, shown shortly in Table 2) were selected at random and one female subject (subject 3, shown shortly in Table 2) was selected because her skin and skull were by far thinner than those of the other subjects. The values of μ_a and μ_s' for the scalp, skull, CSF, and brain shown in Table 1 were used as the initial values for the calculation in subject 1. These values were chosen based on reports from the literature.[16,24] Table 2 shows thickness of each layer in the three subjects, the values of which were used in the head models. The analytical solution derived from the photon diffusion equation for a homogeneous medium in the semiinfinite geometry was fitted to the TPSF obtained from Monte Carlo (MC) simulation to estimate the mean μ_a and mean μ_s' for the head model, in which it was assumed that this head model was a semiinfinite homogeneous medium. These estimated mean μ_a and mean μ_s' (MC-μ_a, MC-μ_s') were compared with the mean μ_a and mean μ_s' at 759 nm obtained from time-resolved measurement (TRS-μ_a, TRS-μ_s') in each subject. When the MC values were not equal to the TRS values, one of the eight parameters (μ_a and μ_s' for four layers) was changed one at a time by every 0.002 or 0.003 for μ_a and by every 0.1 or 0.2 for μ_s'. Applying a new value of the optical properties to the head model, we repeated the same procedure until the MC values became equal to the TRS values. In the case of subject 1, for example, we first altered the μ_a of the scalp from 0.01 to 0.012, 0.015, 0.018, and 0.02. Then, the μ_a of the skull was changed, in which a new μ_a

Table 2 Thickness of the scalp, skull, and CSF in three subjects.

	Age (y)	Sex	Scalp (mm)	Skull (mm)	CSF (mm)
Subject 1 (the upper occipital region)	22	male	7.8	6.7	0.8
Subject 2 (the right frontal region)	21	male	5.4	6.3	0.5
Subject 3 (the left frontal region)	39	female	3.6	4.3	1.5

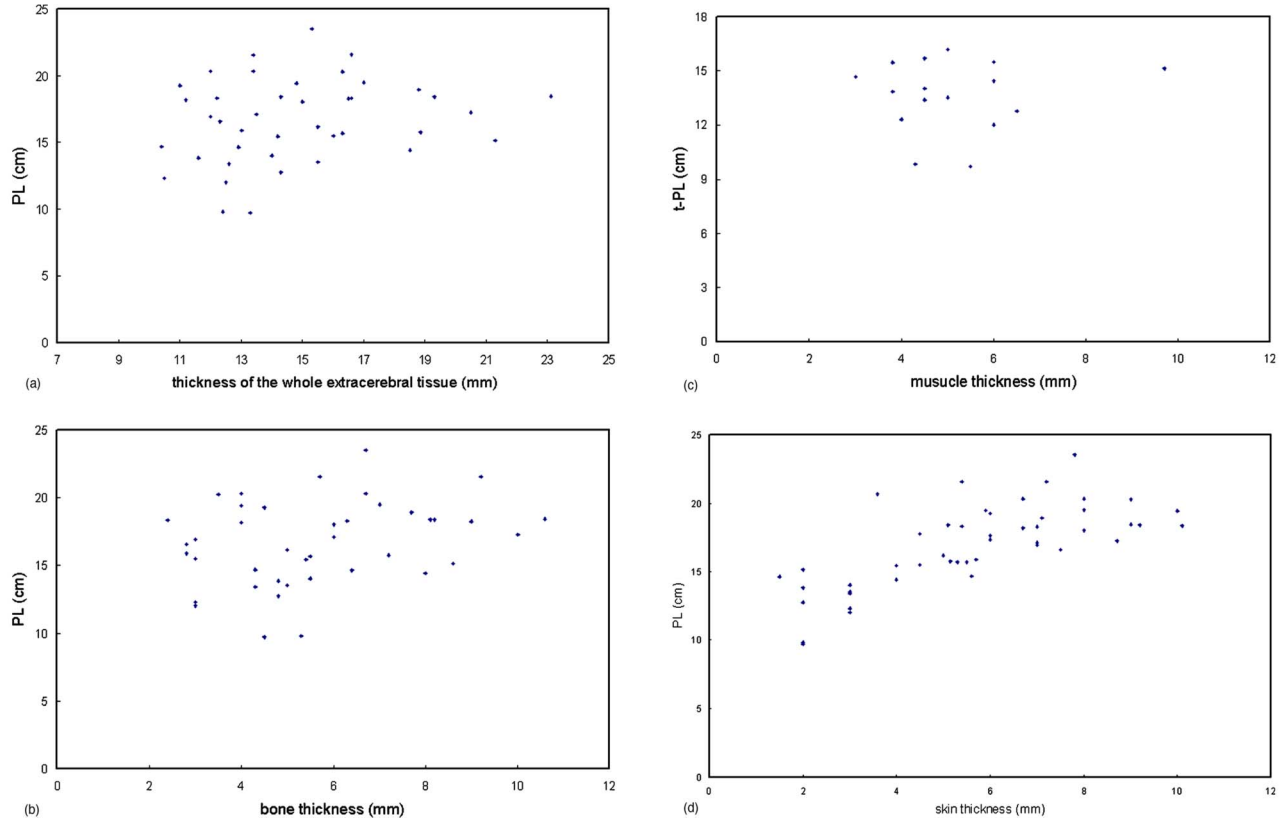

Fig. 4 Relationship between the PL and thickness of (a) the whole extracerebral tissue, (b) skull, (c) muscle, and (d) scalp.

value of the scalp was applied (0.012, 0.015, or 0.018). After 23 combinations were tested, the optical properties were determined in subject 1.

We measured one position by TRS five times and calculated the mean values and standard deviation (SD) of TRS-μ_a and TRS-μ_s'. When the MC values were within the mean ±SD of the TRS values, the MC values were considered to be equal to the TRS values. Reproducibility and statistical variations of measuring optical properties by the TRS-10 were examined by measuring the solid phantom of polyoxymethylene at the same position 100 times: TRS-μ_a=0.0007±0.00002 mm^{-1}, TRS-μ_s'=0.946±0.002 mm^{-1} (mean ±SD). The determined values for subject 1 were used as the initial values for subjects 2 and 3. To confirm the uniqueness of solutions, we tested more than 10 other combinations within the maximum and minimum variations for μ_a and μ_s' employed in the process of solving inverse problems and found no solutions.

2.5 *Estimation of p-PLs*

Applying the optical properties determined in the preceding session to each subject's head model, we first calculated the light attenuation (A). Then, an attenuation change (ΔA) caused by increasing the μ_a for the brain ($\mu_{a\ \mathrm{brain}}$) by 0.002 mm^{-1} was estimated. If the absorption by the brain is changed, the change in the intensity of the detected light can be described[25] by $\Delta A \approx \text{p-PL} \cdot \Delta\mu_{a\ \mathrm{brain}}$. Thus, the p-PL is estimated by $\Delta A / \Delta\mu_{a\ \mathrm{brain}}$. To examine the relationship between the PL and the p-PL, the scalp and skull thickness of each head model were changed, while the CSF thickness was fixed at 1 mm, scalp thickness was 3 or 5 mm, and skull thickness was 3, 5, 7, or 9 mm. For each combination of scalp and skull thicknesses, we estimated the PLs from the corresponding TPSF and the p-PLs by the same procedure just described.

3 Results

3.1 *Relationship Between the PL and Thickness of the Scalp, Skull, Muscle, and the CSF*

Figure 4(a) shows the relationship between the PL and thickness of the whole extracerebral tissue (the scalp, skull, muscle, CSF). No correlation was observed (r^2=0.05). There were no correlations between the PL and thickness of the skull (r^2=0.08) or the muscle (r^2=0.005), either [Figs. 4(b) and 4(c)]. These results indicate that the PL cannot be determined from thickness of the skull, muscle, or extracerebral tissue only. In contrast, the PL was closely related to scalp thickness (r^2=0.52, $p<0.01$) [Fig. 4(d)]. This suggests that the contribution of light that travels within the scalp to the whole detected light is rather large.

3.2 *Optical Properties in the Head*

Table 3 shows the optical properties of the scalp, skull, CSF, and brain at 759 nm determined by solving inverse problems in the three subjects. The μ_a values for all the layers were the same in the three subjects except for the brain in subject 2, which was 0.03 mm^{-1}; it was 0.02 mm^{-1} in the other two subjects. The μ_s' for the scalp varied with each subject (1.1,

Table 3 Optical properties of each layer of the head at 759 nm in subjects 1, 2, and 3.

	μ_a (mm^{-1})			μ_s' (mm^{-1})		
Layer	Subject 1	Subject 2	Subject 3	Subject 1	Subject 2	Subject 3
Scalp	0.015	0.015	0.015	1.3	1.1	2.0
Skull	0.012	0.012	0.012	1.0	0.8	1.0
CSF	0.0033	0.0033	0.0033	0.1	0.1	0.1
Brain	0.02	0.03	0.02	1.7	1.7	1.7

1.3, 2.0 mm^{-1}), though the μ_s' values for the other layers were the same except for the skull in subject 2, which was 0.8 mm^{-1}, while it was 1.0 mm^{-1} in subjects 2 and 3.

Table 4 shows mean μ_a and mean μ_s' for the three subjects' heads that were estimated by MC simulations by the use of the optical properties shown in Table 3. All the MC-μ_a and MC-μ_s' values were within the mean values of TRS-μ_a and TRS-μ_s' ± SD. Figure 5 shows the TPSF obtained from the MC simulation, which corresponded to the deconvoluted TPSF obtained from the TRS measurement on subject 3.

Twenty-three iterative processes were performed to determine the optical properties in subject 1, while five and eight processes were performed for subjects 2 and 3, respectively. One iterative process took 24 to 32 h. Maximum and minimum variations for μ_a $[\mu_{a,\max}, \mu_{a,\min}]$ employed in these processes were $(0.02, 0.01)$ mm^{-1} for the scalp, $(0.015, 0.008)$ for the skull, and $(0.03, 0.016)$ mm^{-1} for the brain. Maximum and minimum variations for μ_s' $(\mu_{s,\max}', \mu_{s,\min}')$ were $(2.5, 1.0)$ mm^{-1} for the scalp and $(1.5, 0.7)$ mm^{-1} for the skull. There was no necessity to change the μ_s' for the brain and the μ_a and μ_s' for the CSF from the initial values.

Table 4 Optical properties of the head obtained from MC simulations and time-resolved measurement (TRS) at 759 nm.

	MC		TRS	
	Mean μ_a (mm^{-1})	Mean μ_s' (mm^{-1})	Mean μ_a (mm^{-1})	Mean μ_s' (mm^{-1})
Subject 1 (the upper occipital region)	0.0144	1.359	0.0147 ±0.0004	1.360 ±0.016
Subject 2 (the right frontal region)	0.0180	1.173	0.0182 ±0.0002	1.144 ±0.041
Subject 3 (the left frontal region)	0.0161	1.305	0.0161 ±0.0001	1.297 ±0.008

TRS data, mean ± SD.

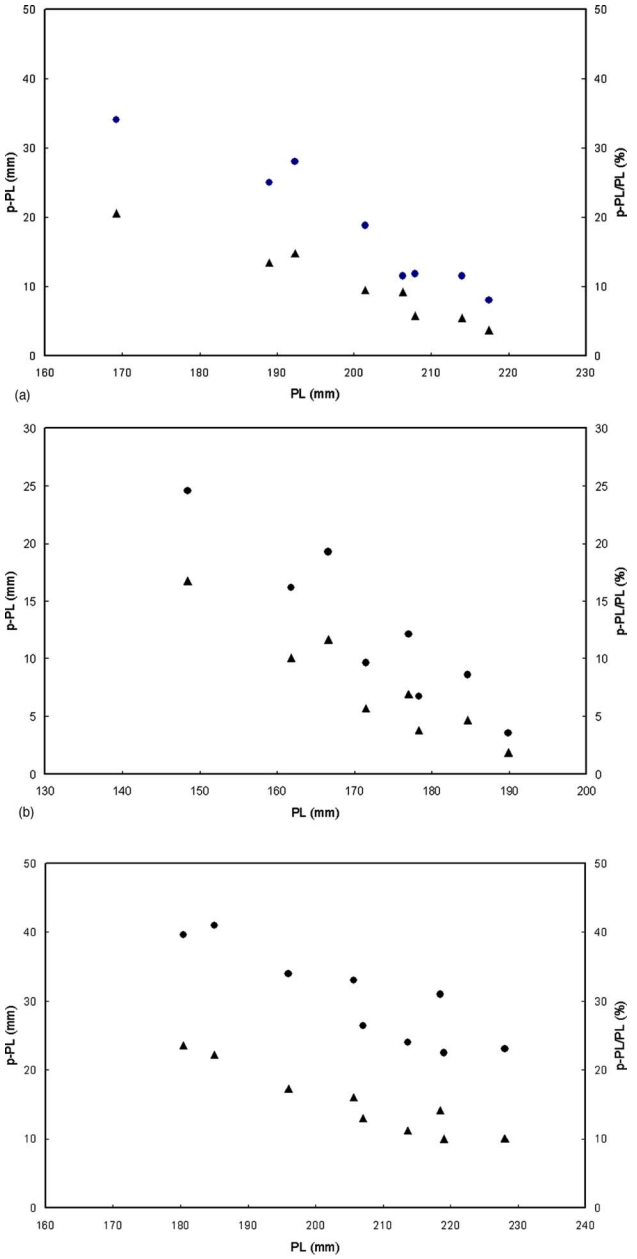

Fig. 6 Relationship between the PL and the p-PL (closed circle) and the ratio of the p-PL to the PL (closed triangle) in the three head models. The optical properties used in (a), (b), and (c) were the same as those of subjects 1, 2, and 3, respectively. Solid circles and solid squares denote p-PL and p-PL/PL, respectively.

3.3 *Relationship Between the PL and p-PL*

Using the optical properties shown in Table 3, the p-PLs were calculated in the three subjects (Table 5). The ratio of the p-PL to the PL was rather small (0.031 to 0.128). Figure 6 shows the relationship between the PL and p-PL for a fixed source detector spacing and the ratio of the p-PL to the PL in the three head models with optical properties shown in Table 3. The p-PL was negatively correlated with the t-PL in all three models, though the slope varied with each model.

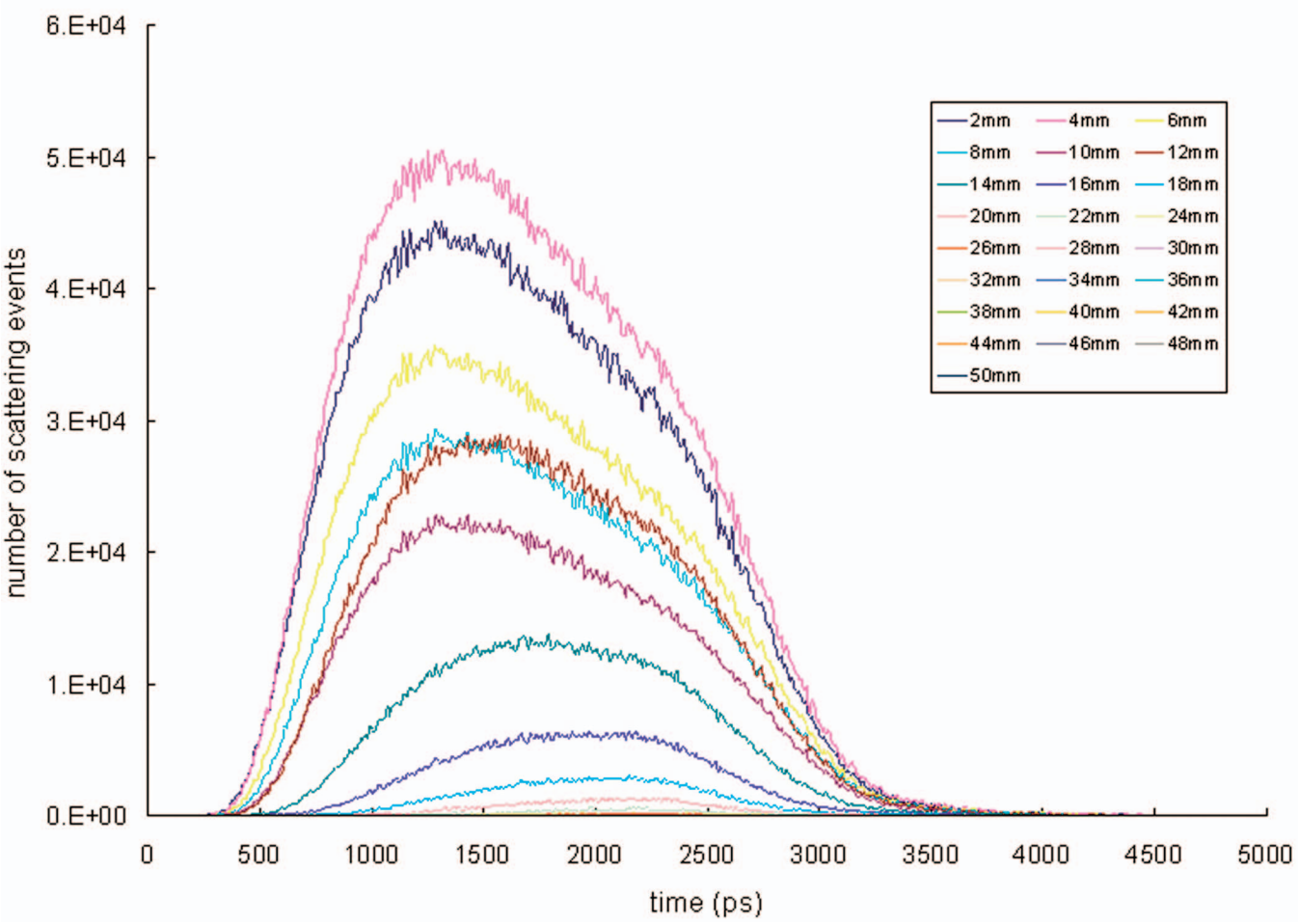

Fig. 7 (a) Number of scattering events in layers ranging from z to $z+1$ mm in depth calculated every 10 ps. (*Continued on next page*)

3.4 *Depth Sensitivity*

Since the thickness of the scalp and skull ranged from about 10 to 15 mm in our subjects, we examined the depth sensitivity in the head models in which the scalp, skull, and CSF thickness were 5, 5, and 1 mm, respectively. The depth sensitivity was defined as the number of detected photons traveling through layers from z to $z+1$ mm in depth and evaluated by the number of scattering events in each thin layer. Figure 7(a) shows the number of scattering events in layers ranging from z to $z+1$ mm in depth calculated every 10 ps in the head model with the same optical properties as those of subject 1 (Table 3). This figure, which shows results every 2 mm of depth, indicates that photons that penetrated into a depth deeper than about 25 mm are hardly detected. Since the number of scattering events in Fig. 7(a) was the summation of scattering events of individual photons within each layer, which was dependent on μ_s' of the corresponding layer, it reflects not only the depth sensitivity but also the μ_s' in each layer. This tendency is obvious in Fig. 7(b): the scattering events suddenly decreased in the CSF and again increased in the surface layer of the brain, which were attributed to lower and higher μ_s' of the CSF and brain, respectively. Since each layer is, however, assumed to be homogeneous in our head models, Fig. 7(b) indicates that the surface layer is most traversed by photons in the brain within a depth of 25 mm from the surface of the scalp. Similar results were obtained from the other models with optical properties of subjects 2 and 3, though the thickness of the scalp in subject 3 was 3 mm.

Table 5 The mean total path length (PL), partial path length in the brain (p-PL), and the ratio of the p-PL to the PL in subjects 1, 2, and 3.

	PL (mm)	p-PL (mm)	p-PL/PL
Subject 1 (the upper occipital region)	219.2	6.85	0.031
Subject 2 (the right frontal region)	184.3	9.15	0.049
Subject 3 (the left frontal region)	206.6	26.4	0.128

4 Discussion

While NIRS is increasingly gaining attention in studies on brain function, the sensitivity of NIRS signals to hemodynamic changes in the brain remains controversial. When the occipital and parietal regions, where the scalp and skull are

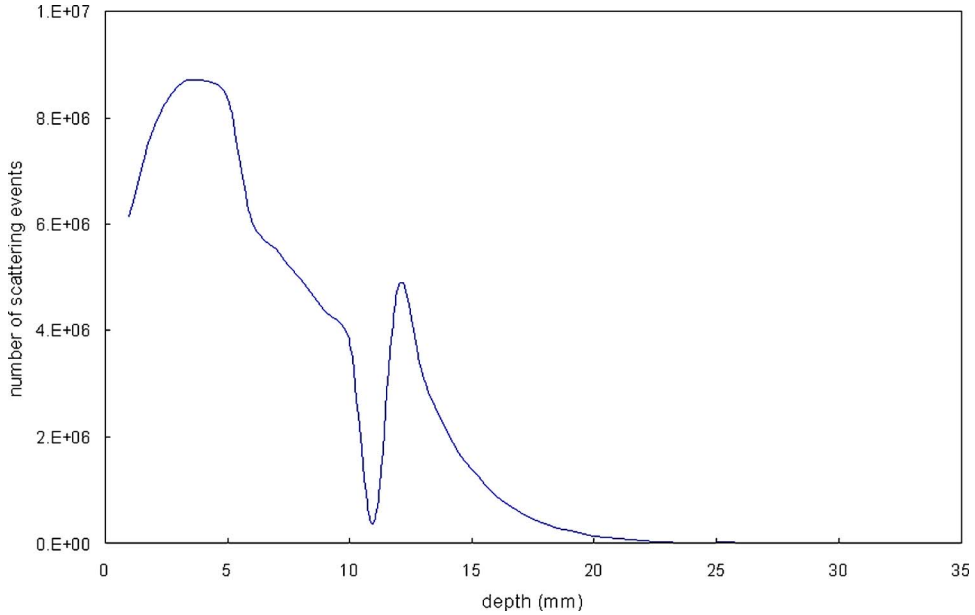

Fig. 7 (*Continued*).
(b) The number of scattering events in each layer in the head model in which the scalp, skull, and CSF were 5, 5, and 1 mm, respectively. The optical properties were the same as those of subject 1.

generally thick, are measured, there is a question whether the detected light actually reached the brain. In addition, the present study has demonstrated that the PL is strongly related to the scalp thickness. This indicates that the contribution of the scalp to the optical path between the source and detector is large, while the contribution of the brain is small. Thus, the estimation of the p-PL is crucial not only for quantification but also for evaluating the sensitivity of NIRS signals to the brain.

Accurate estimation of the p-PL through the use of MC simulation requires realistic head models generated from MRI scans, such as those proposed by Fukui et al.[16] with true optical properties of each layer of the head. Since it was difficult, however, to perform MC simulations on such a realistic model, we employed four-layered slab head models, in which the thickness of each layer was estimated based on the individual MRI scan. The optical properties of the skin, bone, and the brain have been measured by various methods, which were performed on isolated tissues,[26] intraoperatively on humans,[24] or animals.[27] These studies have provided a wide range of values, which can be accounted for by the fact that experimental conditions were different from study to study. Recently, Choi et al. reported on a noninvasive determination of the optical properties of adult human brain by use of a multi-distance frequency domain method.[28] They considered the human head to be a two-layered turbid medium, in which the impact of CSF was expected to be insignificant. By use of MC simulations, however, we confirmed that the influence of the CSF on light propagation cannot be ignored (data not shown), as Okada et al. reported.[29] In addition, our findings that the PL is dependent on the scalp thickness and the optical properties of the scalp are different from that of the skull indicate that a four-layered model is more appropriate for determination of the optical properties of the human head.

Unlike a general approach to the inverse problem, we did not use an iterative algorithm based on the finite element method but carried it out by trial and error. Thus, it took a long time for the MC-μ_a and MC-μ_s' to become equal to the TRS values, especially when we performed MC simulations using the initial values in Table 1. As shown in Fig. 5 and Table 4, however, it was possible to obtain solutions by our approach. The values of the optical properties determined in this study are acceptable compared with published data. Among the three subjects, the μ_s' of the scalp varied with each subject. This can be explained by the fact that the scalp, which consists of multiple histological elements such as the collagen, elastic fibers, and fatty tissues, is more inhomogeneous than the other layers, and contents of these elements are supposed to vary with age and gender. Although our trial-and-error fitting process works properly and determination of μ_a and μ_s' is feasible, we cannot rule out the possibility that a TPFS similar to Fig. 5 is obtained by other different combinations of eight parameters. Barnett et al.[30] recently has reported that the determination of μ_a and μ_s' of a 3-D head model with tissue geometry based on segmented magnetic resonance data from theoretically obtained eight TPSFs. Handling the inverse problem by use of Bayesian inference and introducing a realistic noise model, they predicted coefficient error bars rather than presenting a single best solution. In this study, without inferring CSF properties in their segmented model, six parameters were obtained from eight TPSFs measured with various source-detector spacing. This implies the possibility that the inverse problem in our study does not have a unique solution. Considering the maximum and minimum variations for μ_a and μ_s' employed in our process of solving inverse problems, however, it is unlikely that other combina-

tions, if any, are quite different from the combination determined in the present study.

The p-PLs estimated in the three subjects and the three head models were small: in the head models, 5 to 22% at a differential path length factor[6] (DPF, the ratio of the optical fiber separation to the PL) of 6. This is in accordance with other theoretical analyses, in which different optical properties and head models were used from those in this study.[10,16] For a fixed source detector spacing, the p-PL was negatively correlated with the PL, which is also consistent with the recent theoretical study.[17] Furthermore, the slope of p-PL to PL curve (Fig. 6) varied with optical properties of the head. Thus, comparison of NIRS measurements by cw-type instruments across measurement points is of no significance without estimation of the p-PL.

Figure 7 indicates that light penetrating into the human adult brain deeper than 25 mm from the surface of the scalp is rarely detected, whereas the number of photons that travel through the brain surface layer are the largest among the detected photons penetrating into the brain tissue. Taken together, the results (Table 5 and Figs. 6 and 7) mean that while the contribution of the p-PL to the PL is small, the detected light penetrating into the brain mainly spreads near the brain surface, where the pial arteries lie. This is in agreement with the theoretical analyses by Firbank et al.,[14] though the precise depth sensitivity is expected to vary with the optical properties and the thickness of each layer of the head. It is thus concluded that NIR signals are sensitive to changes occurring in activation-related dilation of the pial arteries, which is supposed to cause a large change in μ_a. This explains why NIRS can detect focal brain activation, even though the main light path is within the extracerebral tissue. However, it is open to question whether it holds in a case where blood flow changes occur in both the extracerebral and cerebral tissues. Thus, selective detection of the changes attributed to the brain is required, which also overcomes the problems of quantification.

Diffuse optical tomography (DOT), which reconstructs images of Hb concentration changes using multiple light sources and detectors, is a potential technique for quantitative detection of focal changes in cerebral hemodynamics.[31] DOT is not based on the modified Beer-Lambert law and can be performed[32] with TRS, frequency domain instruments,[33] and a cw system.[34] However this technique, which requires multichannel instruments, is still in the developmental stage. TRS is also a potential tool for this purpose. It provides the TPSF, which carries information about depth-dependent attenuation even for a measurement with a single source-detector distance because light that penetrates into deeper positions in the head is detected later. While several approaches with TRS have been proposed,[35–37] further investigation must be continued to apply these methods to human head measurement.

5 Conclusions

Using not only theoretical but also experimental methods, we confirmed previous findings obtained from theoretical methods. The NIRS signal is sensitive to hemodynamic changes associated with the brain activation under the conditions in which hemodynamic changes occurring in the extracerebral tissue is ignorable. The p-PL is negatively related to the PL for a fixed source-detector spacing and its relationship varies with the head geometry. This means that for quantification of NIRS measurements during brain activation, substitution of the PL to the modified Beer-Lambert law leads not only the partial volume error but also invalid results. Comparing amplitudes of NIRS signals across measurement positions is not valid with conventional NIRS instruments based on the modified Beer-Lambert law, unless the p-PL is determined. Thus, to increase the utility of NIRS, future studies should focus on the issues of quantification and separation of signals arising from the cerebral tissue from those in the extracerebral tissue.

Acknowledgments

The authors gratefully acknowledge Professor Yukio Yamada (University of Electro-Communications), Dr. Yutaka Yamashita, and Dr. Motoki Oda (Hamamtsu Photonics KK.) for helpful discussions.

References

1. J. E. Brazy, D. V. Lewis, M. H. Mitnick, and F. F. Jöbsis, "Noninvasive monitoring of cerebral oxygenation in preterm infants: preliminary observations," *Pediatrics* **75**, 217–225 (1985).
2. J. S. Wyatt, M. Cope, D. T. Delpy, S. Wray, and E. O. R. Raynolds, "Quantification of cerebral oxygenation and haemodynamics in sick newborn infants by near infrared spectrophotometry," *Lancet* **ii**, 1063–1066 (1986).
3. Y. Hoshi and M. Tamura, "Detection of dynamic changes in cerebral oxygenation coupled to neuronal function during mental work in man," *Neurosci. Lett.* **150**, 5–8 (1993).
4. A. Villringer, J. Plank, C. Hock, L. Schleikofer, and U. Dirnagl, "Near-infrared spectroscopy (NIRS): a new tool to study hemodynamic changes during activation of brain function in human adults," *Neurosci. Lett.* **154**, 101–104 (1993).
5. F. F. Jöbsis, "Noninvasive infrared monitoring of cerebral and myocardial oxygen sufficiency and circulatory parameters," *Science* **198**, 1264–1267 (1977).
6. D. T. Delpy, M. Cope, P. van der Zee, S. R. Arridge, S. Wray, and J. S. Wyatt, "Estimation of optical pathlength through tissue from direct time of flight measurement," *Phys. Med. Biol.* **33**, 1433–1442 (1988).
7. B. Chance, S. Nioka, J. Kent, K. McCully, M. Fountain, R. Greenfield, and G. Holtom, "Time-resolved spectroscopy of hemoglobin and myoglobin in resting and ischemic muscle," *Anal. Biochem.* **174**, 698–707 (1988).
8. B. Chance, M. Maris, J. Sorge, and M. Z. Zhang, "A phase modulation system for dual wavelength difference spectroscopy of hemoglobin deoxygenation in tissues," *Proc. SPIE* **1204**, 481–491 (1990).
9. J. R. Lakowicz and K. Berndt, "Frequency domain measurement of photon migration in tissues," *Chem. Phys. Lett.* **166**, 246–252 (1990).
10. G. Strangman, M. A. Franceschini, and D. A. Boas, "Factor affecting the accuracy of near-infrared spectroscopy concentration calculations for focal changes in oxygenation parameters," *Neuroimage* **18**, 865–879 (2003).
11. M. S. Patterson, B. Chance, and B. C. Wilson, "Time resolved reflectance and transmittance for the noninvasive measurement of tissue optical properties," *Appl. Opt.* **28**, 2331–2336 (1989).
12. H. Zhao, Y. Tanikawa, F. Gao, Y. Onodera, A. Sassaroli, K. Tanaka, and Y. Yamada, "Maps of optical differential pathlength factor of human adult forehead, somatosensory motor, occipital regions at multi-wavelengths in NIR," *Phys. Med. Biol.* **47**, 1–18 (2002).
13. G. Graton, J. S. Maier, M. Fabiani, W. W. Mantulinm, and E. Graton, "Feasibility of intracranial near-infrared optical scanning," *Psychophysiology* **31**, 211–215 (1994).
14. M. Firbank, E. Okada, and D. T. Delpy, "A theoretical study of the signal contribution of regions of the adult head to near-infrared spectroscopy studies of visual evoked responses," *Neuroimage* **8**, 69–78 (1998).
15. D. A. Boas, J. P. Culver, J. J. Stott, and A. K. Dunn, "Three dimensional Monte Carlo code for photon migration through complex heterogeneous media including the adult human head," *Opt. Express* **10**, 159–170 (2002).

16. Y. Fukui, Y. Ajichi, and E. Okada, "Monte Carlo prediction of near-infrared light propagation in realistic adult and neonatal head models," *Appl. Opt.* **42**, 2881–2887 (2003).
17. E. Okada and D. T. Delpy, "Near-infrared light propagation in an adult head model. II. Effect of superficial tissue thickness on the sensitivity of the near-infrared spectroscopy signal," *Appl. Opt.* **42**, 2915–2922 (2003).
18. M. Oda, Y. Yamashita, T. Nakano, A. Suzuki, K. Shimizu, I. Hirano, F. Shimomura, E. Ohmae, T. Suzuki, and Y. Tsuchiya, "Near-infrared time-resolved spectroscopy system for tissue oxygenation monitor," *Proc. SPIE* **3597**, 611–617 (1999).
19. H. Zhang, M. Miwa, T. Urakami, Y. Yamashita, and Y. Tsuchiya, "Simple subtraction method for determining the mean path length traveled by photons in turbid media," *Jpn. J. Appl. Phys.* **37**, 700–704 (1998).
20. M. S. Patterson, S. J. Madsen, J. D. Moulton, and B. C. Wilson, "Diffusion equation representation of photon migration in tissue," in *IEEE 1991 Microwave Symp. Digest*, pp. 905–908 (1991).
21. P. B. Bevington, "*Data Reduction and Error Analysis for the Physical Sciences*," McGraw-Hill, New York (1969).
22. V. D. O'Connor and D. Phillips, "*Time-Correlated Single-Photon Counting*," Academic Press, London (1985).
23. L. Wang and S. L. Jacques, "MCML-Monte Carlo modeling of light transport in multi-layered tissues," *Comput. Methods Programs Biomed.* **47**, 131–146 (1995).
24. F. Bevilacqua, D. Piguet, P. Marquet, J. D. Gross, B. J. Tromberg, and C. Depeursige, "*In vivo* local determination of tissue optical properties: applications to human brain," *Appl. Opt.* **38**, 4939–4950 (1999).
25. M. Hiraoka, M. Firbank, M. Essenpreis, M. Cope, S. R. Arridge, P. van der Zee, and D. T. Delpy, "A Monte Carlo investigation of optical pathlength in inhomogeneous tissue and its application to near-infrared spectroscopy," *Phys. Med. Biol.* **38**, 1859–1876 (1993).
26. C. R. Simpson, M. Kohl, M. Essenpreis, and M. Cope, "Near-infrared optical properties of ex vivo human skin and subcutaneous tissues measured using the Monte Carlo inversion technique," *Phys. Med. Biol.* **43**, 2465–2478 (1998).
27. A. Sassaroli, F. Martelli, Y. Tanikawa, K. Tanaka, R. Araki, Y. Onodera, and Y. Yamada, "Time-resolved measurement of in vivo optical properties of piglet brain," *Opt. Rev.* **7**, 420–425 (2000).
28. J. Choi, M. Wolf, V. Toronov, U. Wolf, C. Polzonetti, D. Hueber, L. P. Safonova, R. Gupta, A. Michalos, W. Mantulin, and E. Gratton, "Noninvasive determination of the optical properties of adult brain: near-infrared spectroscopy approach," *J. Biomed. Opt.* **9**, 221–229 (2004).
29. E. Okada, M. Firbank, M. Schweiger, S. R. Arridge, M. Cope, and D. T. Delpy, "Theoretical and experimental investigation of near-infrared light propagation in a model of the adult head," *Appl. Opt.* **36**, 21–31 (1997).
30. A. H. Barnett, J. P. Culver, A. G. Sorensen, A. Dale, and D. A. Boas, "Robust inference of baseline optical properties of the human head with three-dimensional segmentation from magnetic resonance imaging," *Appl. Opt.* **42**, 3095–3108 (2003).
31. S. R. Arridge, "Optical tomography in medical imaging," *Inverse Probl.* **15**, R41–R93 (1999).
32. F. Gao, H. Zhao, and Y. Yamada, "Improvement of image quality in diffuse optical tomography using full time-resolved data," *Appl. Opt.* **41**, 778–791 (2002).
33. B. W. Pogue, M. S. Patterson, H. Jiang, and K. D. Paulsen, "Initial assessment of a simple system for frequency domain diffuse optical tomography," *Phys. Med. Biol.* **40**, 1709–1729 (1995).
34. D. Boas, A. M. Dale, and M. A. Franceschini, "Diffuse optical imaging of brain activation: approaches to optimizing image sensitivity, resolution, and accuracy," *Neuroimage* **23**, S275–S288 (2004).
35. A. H. Hielscher, H. Liu, B. Chance, F. K. Tittel, and S. L. Jacques, "Time-resolved photon emission from layered turbid media," *Appl. Opt.* **35**, 719–728 (1996).
36. J. Steinbrink, H. Wabnitz, H. Obrig, A. Villringer, and H. Rinneberg, "Determining changes in NIR absorption using a layered model of the human head," *Phys. Med. Biol.* **46**, 879–896 (2001).
37. M. Shimada, Y. Hoshi, and Y. Yamada, "A simple algorithm for measurement of the absorption coefficients of a two-layered medium by spatially and time-resolved reflectance," *Appl. Opt.* **44**(35), 7554–7563 (2005).